JMEPEG
https://doi.org/10.1007/s11665-025-11857-4

1059-9495/$19.00

ORIGINAL RESEARCH ARTICLE

Synergistic Strengthening: Tailoring Microstructure and Maximizing Dry Sliding Wear Resistance in Al-Ni Alloys

V. Jayaseelan, S. Sambath, M.R. Anantha Padmanaban, and VijayAnanth Suyamburajan

Submitted: 4 March 2025 / Revised: 1 May 2025 / Accepted: 30 May 2025

Lightweight and durable materials like Al-Ni alloys are needed for applications demanding high-strength-to-weight ratios, such as in the automotive and aerospace industries. This study investigated the microstructural evolution and mechanical properties of stir cast Al-Ni alloys (5-7 wt.% Ni) and optimized their dry sliding wear behavior using the Taguchi-Gray relational analysis. Increasing nickel content led to a higher volume fraction of the hard Al_3Ni intermetallic phase, confirmed by XRD and EDS analyses. This resulted in a 2.6% increase in ultimate tensile strength (Al-7 wt.% Ni compared to Al-5 wt.% Ni). Increasing the nickel content in the stir cast Al-Ni alloys resulted in enhanced hardness, with the Al-7 wt.% Ni alloy exhibiting a 3.37% higher hardness than the Al-5 wt.% Ni alloy, primarily attributed to the formation of hard Al_3Ni intermetallics and solid solution strengthening. The density also slightly increased with higher Ni content due to the substitution of Al atoms with heavier Ni atoms. Sliding distance and applied load were identified as the most significant factors affecting wear, while nickel content had a less dominant influence. Multi-objective optimization resulted in a 14.1% improvement in dry sliding performance, with the gray relational grade improving by 86.8% from the initial to the optimal wear test settings. This study highlights the positive correlation between microstructural features, mechanical properties, and wear resistance in Al-Ni alloys.

Keywords Al-Ni alloys, dry sliding wear, gray relational analysis, microstructure, mechanical properties, Taguchi

1. Introduction

The low density, high specific strength, and superior corrosion resistance of aluminum-based alloys make them ideal for a broad range of industrial uses (Ref 1). As their name implies, binary aluminum alloys have been formulated from aluminum and one other alloying element. Because of their superior properties compared to pure aluminum, binary aluminum alloys are important materials for many industrial applications (Ref 2). As a result, Al-Si alloys are widely used for good casting characteristics, automotive/engine components, and other automotive parts that require good weldability and corrosion resistance (Ref 3). Heat-treatable, high-strength/low-weight Al-Cu alloys are used in aerospace components, bicycle frames, and structural parts. Exceptional corrosion resistance, especially in marine environments, is shown by Al-Mg alloys, which are found applicable in boat hulls, aircraft structures, beverage cans, and so on. While Al-Mn alloys provide a combination of strength, ductility, and corrosion resistance, they are suited for architectural applications such as window frames and roofing sheets (Ref 4). Lastly, Al-Ni alloys are known for high wear resistance and high-temperature strength and are used for severe sliding contact applications such as bearings and gears (Ref 5). For a particular binary aluminum alloy, the properties required and the desired application dictate the choice. Al-Ni has been relatively unexplored compared to other binary aluminum alloys for their ability to enhance the wear resistance of components exposed to sliding contact (Ref 6). While these alloys have a very high wear rate under dry sliding conditions, they are not widely used within the transportation industry (Ref 7).

The presence of hard intermetallic compounds like Al_3Ni and Al-Ni accounts for their high hardness and wear resistance of binary Al-Ni alloys (Ref 8, 9). At the same time, Al-Ni alloys exhibit good high-temperature strength and are applicable in severe applications such as engine components and turbine blades. Despite their higher cost and greater difficulty of processing than other aluminum alloys, the combination of wear resistance and high-temperature strength of these alloys is essential for applications where they are essential (Ref 10). Al_3Ni intermetallic has an inherent hardness greater than the surrounding aluminum matrix, and as such, the alloy resists deformation and abrasion (Ref 11). Al_3Ni forms a heterogeneous microstructure with hard phases present and dispersed into softer aluminum, which functions as barriers to block wear

V. Jayaseelan, Department of Mechanical Engineering, Saveetha Engineering College, Chennai 602105, India; **S. Sambath**, Department of Mechanical Engineering, SRM Madurai College for Engineering and Technology, Sivaganga 630612, India; **M.R. Anantha Padmanaban**, Department of Mechanical Engineering, Saranathan College of Engineering, Tiruchirapalli 620012, India; and **VijayAnanth Suyamburajan**, Department of Mechanical Engineering, VELS Institute of Science, Technology & Advanced Studies, Chennai 600117, India. Contact e-mail: jaiseelanv@gmail.com.

Published online: 28 August 2025

track propagation. Furthermore, the high-temperature strength of these alloys is provided by the Al_3Ni, which has a higher melting point than the base metal, permitting these alloys to retain a high strength and wear resistance at elevated temperatures (Ref 12). Yet, it should be pointed out that even though they do increase the wear resistance, Al_3Ni can reduce the ductility of the alloy and thus make them potentially less tolerant to deformation before fracture. Al-Ni alloys can be classified into three types based on their nickel content: eutectic, hypoeutectic, and hypereutectic. For example, eutectic Al-Ni alloys with a Ni content of 6.1 wt.% solidify at a single temperature (639.9ºC) to produce a fine lamellar structure of aluminum and Al_3Ni with good castability, improved wear resistance, and reasonable strength (Ref 13). For hypoeutectic alloys with less than 6.1 wt.% Ni, primary aluminum dendrites surrounded by the eutectic structure yield good ductility and moderate wear resistance. The hypereutectic alloys (more than 6.1 wt.% Ni) solidify primary Al_3Ni crystals first, then the eutectic structure, which exhibits lower ductility but higher wear resistance and strength. The selection of hypoeutectic, hypereutectic, or eutectic alloys depends on the needs of the specific application, requiring reasonable ductility, better wear resistance, and strength, or the best balance of properties and good castability, respectively (Ref 14). Binary Al-Ni alloys can be manufactured by a low-cost and versatile process such as stir casting. This technique involves mechanically stirring molten metal to achieve homogeneous alloying element distribution, resulting in a refined and uniform microstructure (Ref 15). The advantages of this place-out processing are that it is possible to make near-net-shape components, allow good control of the microstructure, and potentially scale up to meet the needs of industrial applications of these wear-resistant Al-Ni alloys (Ref 16).

Studying the dry sliding wear behavior of Al-Ni alloys, such as bearings and gears, is crucial due to their increasing use in wear resistance applications. In order to predict their lifespan and optimize their performance in the absence of lubrication or under limited lubrication and dry sliding conditions, it is therefore important to understand how these alloys respond to such conditions. The properties with respect to the microstructure of Al-Ni alloys as given in this review do not deal directly with the importance of the estimation of the dry sliding wear behavior of them (Ref 17, 18). However, since such sources are focused on wear resistance and hard intermetallic compounds such as Al_3Ni were detected, this research is needed. Through study of wear, it is possible to optimize alloy composition, microstructure, and processing parameters in search of improved wear resistance (Ref 19). Take, for example, how these can help inform the development of alloys with further improved properties by elucidating the role of Al_3Ni distribution and morphology in wear resistance.

As stated earlier, a dry sliding wear study of Al-Ni alloys is important for predicting real-world performance, material design and optimization, cost reduction and efficiency improvements, and the creation of new applications. Understanding wear mechanisms under specific combinations of dry sliding conditions is important for the more accurate prediction of lifespans and for improving wear resistance by optimizing alloy composition, microstructure, and processing (Ref 20). By nature, mitigating wear will result in lower maintenance costs and increased system efficiency. With growing knowledge of dry sliding wear in Al-Ni alloys, their use in novel, demanding applications where high wear resistance is needed may be of interest. In short, understanding the dry sliding wear behavior of Al-Ni alloys is important to further push the application and development of Al-Ni alloys to different industries.

Fabrication of Al-Ni alloy prepared by stir casting is on the verge in the area of wear-resistant applications such as bearings, gears, etc. In order to optimize their dry sliding wear behavior, however, one must understand the complex interplay between fabrication and application factors (Ref 21). This optimization is necessary to increase wear resistance, tailor alloy properties to meet application requirements, and offer cost-effective solutions. Although it has attracted increasing attention, a research gap exists in the multi-objective optimization of stir cast Al-Ni alloy systems under dry sliding wear. This gap involves few studies of simultaneous optimization of multiple wear characteristics without the consideration of synergistic effects between control factors and no application-specific optimization. A novel innovation is provided by the application of a Taguchi-Gray Relational Approach (GRA) for a systematic experimental design, for considering the complex relationships among multiple wear responses, and for the holistic optimization using dry sliding conditions. Starting from this approach, it is possible to develop high-performance Al-Ni alloys with a controlled wear resistance efficiency for specific applications. Thus, in this work, the dry sliding wear resistance of three different Al-Ni alloys with different nickel content (5 to 7 wt.%) has been investigated for the first time, and wear test factors have been optimized to give better wear resistance. The goal was to develop a systematic approach to simultaneously optimize multiple wear characteristics of these stir cast Al-Ni alloys.

2. Experimental and Statistical Procedure

2.1 Manufacturing of Al-Ni Alloys

Al-Ni alloy cast specimens with three different nickel contents (5, 6, and 7 wt.%) were fabricated using the stir casting process. The compositions were chosen to approximately represent hypoeutectic (5 wt.% Ni), eutectic (6 wt.% Ni), and hypereutectic (7 wt.% Ni) Al-Ni alloys: Al-5 wt.% Ni (hypoeutectic), Al-6 wt.% Ni (eutectic), and Al-7 wt.% Ni (hypereutectic) alloys. A Metavision-1008i spectrometer was used to examine the chemical composition of alloys, and the findings are presented in Table 1. Pure nickel (Ni) powders were added in the calculated amount to a graphite crucible, which was then placed in a stir cast electric muffle furnace. The furnace temperature was set to 1500 °C with a heating rate of 300 °C/h, and the materials were held at this temperature for 30 minutes. Once the furnace reached the preset temperature, the pure nickel in the graphite crucible completely transformed into

Table 1 Elemental composition of Al-Ni alloys

	Elements, wt,%	
Alloy prepared	**Al**	**Ni**
Al-5 wt.% Ni	94.97	5.03
Al-6 wt.% Ni	93.9	6.1
Al-7 wt.% Ni	92.93	7.07

a molten metal state. In this situation, the pure aluminum ingots were added into the molten bath. After stirring the molten materials, the melt was poured into a permanent graphite mold (as per standard: ASTM B108/B108M-08) and allowed to cool in air. The resulting cast ingots were then used for various characterizations. A cover flux was used to avoid oxidation during melting, and 1 wt.% hexachloroethane tablets were immersed to degas the melt. Figure 1 displays the comprehensive strategy for the inquiry.

2.2 Characterization of Al-Ni Alloys

The microstructure of all three-stir cast Al-Ni specimens was analyzed using a scanning electron microscope (SEM)/electron-dispersive spectroscopy (EDS) that provides detailed insights into the microstructural features of the alloys, including the distribution and morphology of the constituent phases. To carry out the characterizations, a wire electric discharge machine (WEDM) was used to cut each specimen (170 × 70 × 15 mm), and samples of varying sizes were prepared in accordance with ASTM standards discussed below. To detect microstructural characteristics and identify components contained in the processed samples, a ZEISS EVO 18 SEM with EDS was used. Before SEM analysis, cubical samples (10 mm) cut from all stir cast bars were mirror polished using grit papers coated with SiC. Then, at room temperature, they were etched using Keller's reagent (1 mL HF, 1.5 mL HCl, 2.5 mL HNO_3, and 95 mL H_2O), as is standard procedure in metallography. The experimental density of the samples was determined using Archimedes' principle and the weight loss method. The theoretical density was calculated based on the rule of mixtures. A comparison between experimental and theoretical density values was performed to evaluate the effectiveness of the stir casting process for the investigated Al-Ni alloys. Brinell hardness testing was conducted using a BRINELL AKB 3000 tester, employing a 5-mm diameter steel ball indenter and applying a load of 250 kg for 15 s, as per the ASTM E10 standard. The final hardness values considered are the average of five repetitions measured at different spots in the sample. Tensile tests were conducted for the Al-Ni alloys in accordance with the ASTM: B-557M standard. A computerized universal testing machine was used to determine the tensile strength of the alloys at a temperature of 30 °C with a strain rate of 0.01/s. Tensile test specimens were prepared from each alloy using wire EDM, with a gauge length of 100 mm. The specimens were attached between two movable grips containing a strain gauge extensometer, and the tests were performed at a constant cross-head speed. Specimens were tested for their elongation and maximum load-bearing capability. For each alloy, three specimens were used for measuring the tensile properties.

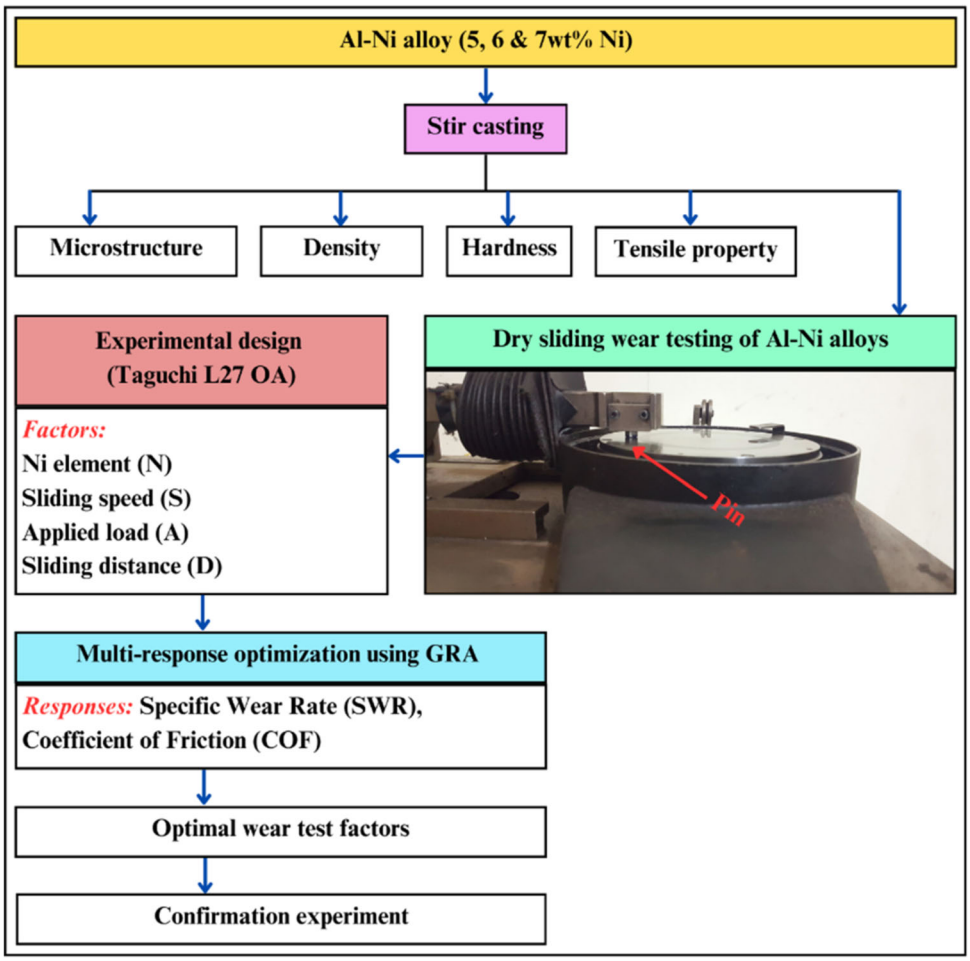

Fig. 1 Schematic illustration of the steps followed in this study

2.3 Dry Sliding Wear Tests

Wear tests were conducted on a pin-on-disk apparatus as per the ASTM G99 standard (Fig. 1) in dry conditions. Cylindrical specimens (6 mm diameter), 10 mm in length, were cut from the stir cast Al-Ni alloys using WEDM. The wear tester was used to conduct dry sliding wear testing at room temperature in compliance with ASTM G99-05. A rotating disk of EN31 steel with a hardness of 60 HRC was used to press the pin specimens of the three Al-Ni alloys. Different sliding speeds, applied loads, and sliding distances were used in the testing. Table 2 lists the control factors taken into account in this study along with their levels. An electronic scale was used to measure the weight of the wear test pins before and after the tests. Additionally, the surface of the counterface was carefully cleaned using acetone prior to testing. SEM was employed to investigate the worn surfaces of all the wear pins. The following Eq 1 was used to calculate the specific wear rate (SWR) (Ref 22).

$$\mathrm{SWR} = \frac{\mathrm{WL}}{(L \times \rho \times SD)} \quad \text{(Eq 1)}$$

where, WL is weight loss, ρ is density of the material, L is load acting on the pin and SD is the sliding distance. Furthermore, coefficient of friction (COF) measurements were included in this study in order to develop a more complete picture of the tribological behavior of these Al-Ni alloys.

2.4 Optimization Technique

Optimizing the two wear responses (SWR and COF) of the stir cast Al-Ni alloys was achieved in the research by using the Taguchi method, a rigorous experimental design tool. The Taguchi method has its capability for wide application to handle complex relationships among multiple variables and in optimizing dry sliding conditions (Ref 23). With only 27 experimental runs, this optimization research was able to examine four control parameters at three levels each, according to the Taguchi L27 orthogonal array. This design is efficient and leads to fewer experimental treatments as compared to a full factorial design. The control variables in this study are the stir cast Al-Ni alloy nickel content (5, 6, and 7 wt.%), sliding speed (1, 2, and 3 m/s), applied load (10, 20, and 30 N), and sliding distance (500, 1000, and 1500 m). The specific wear rate and the coefficient of friction were selected as responses and were optimized simultaneously through the Taguchi-gray relational analysis (GRA) approach. Analysis and determination of optimal control factor settings were done using Minitab 16 statistical software.

The aim of GRA is to derive a single performance criterion called the gray relational grade from the multiple wear responses so that all responses are concurrently optimized (Ref 24). The procedure for this approach is as follows: After the collection of data from the experimental plan for wear tests using the Taguchi L27, normalization, which is considered an essential preprocessing step, is performed. This is important because SWR is measured in one unit and COF is a dimensionless entity; hence, it is not possible to correlate them directly. Using Eq 2, these values are normalized to values that exist in a comparable range, usually 0 and 1. As lower values of SWR and COF are desired for enhanced wear resistance, a smaller-the-better normalization technique is used in this work. This guarantees that subsequent analysis will weigh both responses equally so that neither one overpowers the other.

$$\text{Normalized value } (L_M(N)) = \frac{\max L_M^{\circ}(N) - L_M^{\circ}(N)}{\max L_M^{\circ}(N) - \min L_M^{\circ}(N)} \quad \text{(Eq 2)}$$

where, $L_M^{\circ}(N)$ indicates original data, $\max L_M^{\circ}(N)$ shows the maximum among received original datasets and $\min L_M^{\circ}(N)$ shows the minimum among received original datasets. Furthermore, the relationship between the results of each experimental runs and the ideal solution is quantified in terms of gray relational coefficient (GRC) using Eq 3.

For each response and each experiment:

For each response and each experiment :

$$\xi_M(N) = \frac{\Delta_{\min} + \xi\Delta_{\max}}{\Delta_{oM}(N) + \xi\Delta_{\max}} \quad \text{(Eq 3)}$$

The distinguishing coefficient (ξ) is bounded between 0 and 1, and $\Delta_{\min}$ and $\Delta_{\max}$ are the minimal and maximal deviations of the response, respectively. Further, $\Delta_{oM}(N)$ is the deviation sequence for each and every experiment and it can be calculated using Eq 4.

$$\Delta_{oM}(N) = |L_o(N) - L_M(N)| \quad \text{(Eq 4)}$$

By converting the multi-objective optimization challenge into a single-response problem using the gray relational grade (GRG), it is possible to comprehensively evaluate the combined influence of all four control factors on wear performance. The GRG, calculated for each experimental trial using the specific Eq 5, served as a single metric representing the overall quality of each experimental run (Ref 25).

$$\gamma_M = \frac{1}{n}\sum_{M=1}^{n} \xi_M(N) \quad \text{(Eq 5)}$$

This comparative assessment validates the effectiveness of the optimization methodology in enhancing the wear resistance of the Al-Ni alloys.

Table 2 Control factors and their levels

Factor	Unit	Levels		
		Level 1	Level 2	Level 3
Ni element	Wt.%	5	6	7
Sliding speed	m/s	1	2	3
Applied load	N	10	20	30
Sliding distance	m	500	1000	1500

3. Results and Discussion

3.1 Microstructural Observation

The microstructural observations of stir cast Al-Ni alloys with varying Ni content provide valuable insights into phase evolution and alloy composition. In the Al-5 wt.% Ni alloy, the microstructure reveals a uniform distribution of fine Al_3Ni intermetallic particles dispersed within an α-Al matrix. The

primary phase is aluminum-rich α-Al, appearing as dendritic structures, while the secondary phase consists of a eutectic mixture of α-Al and Al_3Ni located in the inter-dendritic regions (Fig. 2a). As the Ni content increases to 6 and 7 wt.%, the volume fraction of Al_3Ni intermetallics increases correspondingly. In the Al-6 wt.% Ni alloy, a fully eutectic structure forms, composed of needle-like α-Al and Al_3Ni phases solidifying simultaneously throughout the matrix, with no distinct primary phase present (Fig. 2b). In the Al-7 wt.% Ni alloy, the primary phase is Al_3Ni, which solidifies first and appears as cuboidal particles embedded within the eutectic matrix of α-Al and Al_3Ni (Fig. 2c). Overall, two distinct morphologies of Al_3Ni intermetallics are observed in the fabricated alloys: elongated/needle-like structures and primary cuboidal or orthorhombic blocks. These particles, which typically appear darker in SEM, range in size from 1 to 5 μm in length and 0.2-1 μm in width. A finer and more uniform distribution of Al_3Ni is associated with improved strength and hardness, while larger and clustered particles may act as stress concentrators, potentially reducing ductility. The increase in the volume fraction of Al_3Ni intermetallic compounds in stir cast Al-Ni alloys with increasing nickel content, as revealed by ImageJ analysis tool, can be attributed to the basic principles of solidification and phase formation. As the nickel content increases, an amplified amount of nickel is available in the melt during the solidification process. This leads to the formation of a more volume of the Al_3Ni phase, which precipitates out of the aluminum matrix. Specifically, the Al-5 wt.% Ni alloy exhibited 7.9 vol.% Al_3Ni, which increased to 9.1 vol% for the Al-6 wt.% Ni alloy and further to 11.3 vol.% for the Al-7 wt.% Ni alloy. This represents an increase of 15.2% from the Al-5 wt.% Ni to the Al-6 wt.% Ni alloy and a further increase of 24.2% from the Al-6 wt.% Ni to the Al-7 wt.% Ni alloy (Table 3). This trend clearly demonstrates that increasing the nickel content in the Al-Ni alloy system directly correlates with a higher volume fraction of the Al_3Ni intermetallic phase, which in turn contributes to the enhanced mechanical and wear resistance properties observed in these alloys. The EDS analysis has confirmed the presence of both Al and Ni elements, indicating the formation of the beneficial Al_3Ni intermetallic phase within the alloy microstructure (Fig. 2d). These observations are consistent with the findings reported in the literature (Ref 26). The XRD patterns of the Al-Ni alloys reveal that as the Ni content increases, the intensity of the Al peaks decreases, indicating a reduced Al phase, while the intensity of the Al_3Ni intermetallic compound peaks increases, suggesting a higher volume fraction of this phase (Ref 27). The Al-5 wt.% Ni alloy shows a dominant Al phase with a small amount of Al_3Ni, while in the Al-6 wt.% Ni and Al-7 wt.% Ni alloys, the Al_3Ni phase becomes more prominent, with a further increase in its volume fraction (Fig. 3). The most prominent Al peaks are observed around 38° (111), 38.5° (111), 44.7° (200),

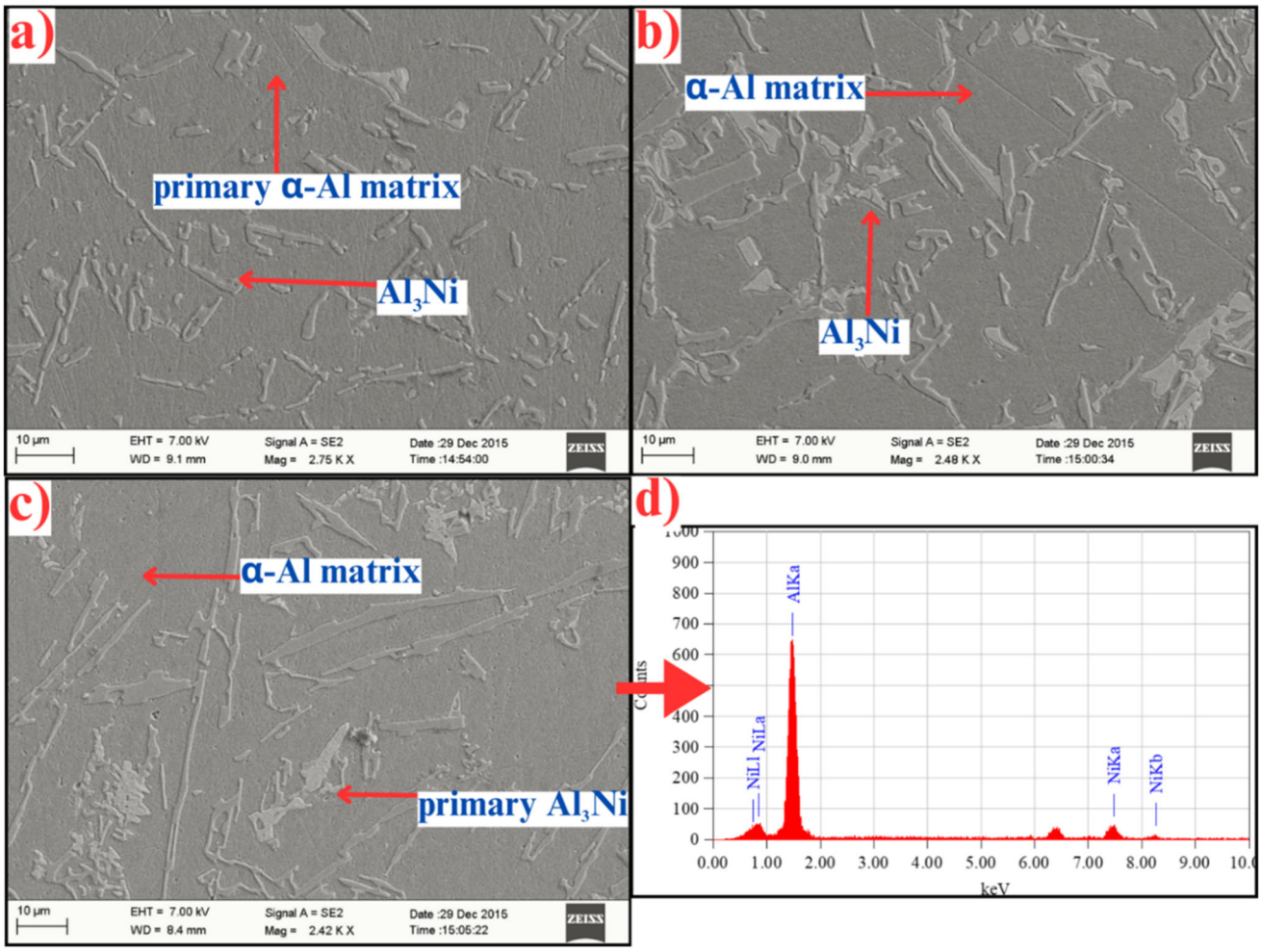

Fig. 2 SEM images of (a) Al-5 wt.% Ni alloy, (b) Al-6 wt.% Ni alloy, (c) Al-7 wt.% Ni alloy, and (d) EDS observation of Al-7 wt.% Ni alloy

Table 3 The observed results of density, tensile and hardness tests

Specimen designation	Experimental density, g/cc	Theoretical density, g/cc	Hardness, BHN	Volume fraction of Al_3Ni, Vol.%	Tensile properties		
					Ultimate tensile strength, N/mm^2	Yield strength, N/mm^2	Elongation, %
Al-5 wt.% Ni alloy	2.715	2.745	89	7.9	143.802	120.666	3.6
Al-6 wt.% Ni alloy	2.719	2.751	91	9.1	144.251	121.360	3.6
Al-7 wt.% Ni alloy	2.726	2.763	92	11.3	147.546	122.984	3.5

65.1° (220), 69° (311), 78.2° (311), and 83° (222), while the strong Al_3Ni peaks are potentially around 37° (111), 43° (200), 50° (200), 60° (220), 64° (220), and 76° (222), with the relative peak intensities depending on factors like cooling rate and microstructure.

3.2 Properties of Al-Ni Alloys

The density values of the stir cast Al-Ni alloys show a slight increase with rising Ni content. This can be attributed to the higher atomic weight of Ni compared to aluminum. Specifically, the Al-6 wt.% Ni alloy is 0.15% denser than the Al-5 wt.% Ni alloy, while the Al-7 wt.% Ni alloy is 0.26% denser than the Al-6 wt.% Ni alloy (Table 3). Atomic weight and density are closely related. Nickel has a higher atomic weight (58.69 g/mol) than aluminum (26.98 g/mol), meaning that a nickel atom is heavier than an aluminum atom (Ref 28). The density of a material is its mass per unit of volume, and when substituting heavier nickel atoms for lighter aluminum atoms in the alloy's crystal structure, the overall mass within the same volume increases, leading to higher density. At these relatively low nickel concentrations, nickel likely dissolves into the aluminum matrix, forming a solid solution. This means that the nickel atoms occupy positions within the aluminum crystal lattice. The size difference between nickel and aluminum atoms determines whether nickel atoms occupy interstitial sites or substitutional sites. Given that nickel atoms are smaller than aluminum atoms, they are more likely to occupy substitutional sites. The density increase is accompanied by beneficial changes in material properties. It is well known that nickel enhances the hardness and strength of aluminum alloys via the emergence of the Al_3Ni intermetallic phase, as shown by XRD analysis. This is because the Al_3Ni phase acts as a hard, dispersed phase within the softer aluminum matrix, hindering dislocation movement and enhancing mechanical properties (Ref 29).

The comparison between experimental and theoretical densities of Al-Ni alloys (5-7 wt.% Ni) produced via stir casting shows consistently high relative densities ($\sim$ 99%), indicating effective incorporation of Ni and minimal porosity. A slight decrease in relative density with increasing Ni content is attributed to greater formation of Al_3Ni intermetallics, which may reduce melt fluidity and promote micro-porosity. Despite this, the near-theoretical densities confirm that solidification shrinkage and gas entrapment were well controlled, suggesting optimized stirring and casting parameters. Overall, the results demonstrate that stir casting is a reliable method for fabricating dense, well-bonded Al–Ni alloy-based structural components.

The observed trend of increasing hardness with higher nickel content in stir cast Al-Ni alloys can be attributed to several key factors. Primarily, this rise in hardness is linked to the formation of the Al_3Ni intermetallic compound. Al_3Ni is known for its exceptional hardness and strength compared to the parent metals (Ref 30). As the nickel content increases from 5 to 7 wt.%, the volume fraction of the Al_3Ni phase also increases. This higher volume fraction of hard Al_3Ni phases within the aluminum matrix effectively hinders the movement of dislocations, which are responsible for plastic deformation. This resistance to dislocation movement translates to increased hardness. Furthermore, solid solution strengthening also contributes to the observed hardness trend. When nickel dissolves into the aluminum matrix, it creates lattice distortions due to the size difference between nickel and aluminum atoms (Ref 31). These distortions make it more difficult for dislocations to move through the crystal lattice, further increasing the alloy's hardness. The quantitative findings highlight the impact of even small nickel additions. The Al-6 wt.% Ni alloy exhibits a 2.22% higher hardness than the Al-5 wt.% Ni alloy, while the Al-7 wt.% Ni alloy shows a 1.11% increase compared to the Al-6 wt.% Ni alloy (Fig. 4). This suggests that the rate of hardness increase might be tapering off at higher nickel contents, which could be due to factors like the saturation of nickel in the aluminum matrix. The increasing trend with higher nickel content is also consistent with literature, as the increased volume fraction of the hard Al_3Ni intermetallic phase strengthens the material and increases its resistance to indentation (Ref 32).

Further, the observed trends in tensile properties of stir cast Al-Ni alloys align with the expected effects of nickel additions and the resulting microstructural changes. Solid solution strengthening and precipitation hardening are the two main strengthening processes that improve the ultimate tensile strength (UTS) as the nickel concentration increases. As nickel dissolves into the aluminum matrix, it creates lattice distortions, making it more difficult for dislocations to move and thus enhancing the alloy's strength. Additionally, the formation of the Al_3Ni intermetallic compound, as confirmed by the XRD analysis, introduces hard phases within the softer aluminum matrix. These phases act as obstacles to dislocation movement, further improving the UTS (Ref 33). The Al-6 wt.% Ni alloy exhibits a modest 0.31% higher UTS than the Al-5 wt.% Ni alloy, while the higher nickel content in the Al-7 wt.% Ni alloy leads to a more significant 2.3% increase in UTS compared to the Al-6 wt.% Ni alloy (Table 3). This suggests a possible synergistic effect of the strengthening mechanisms at the higher

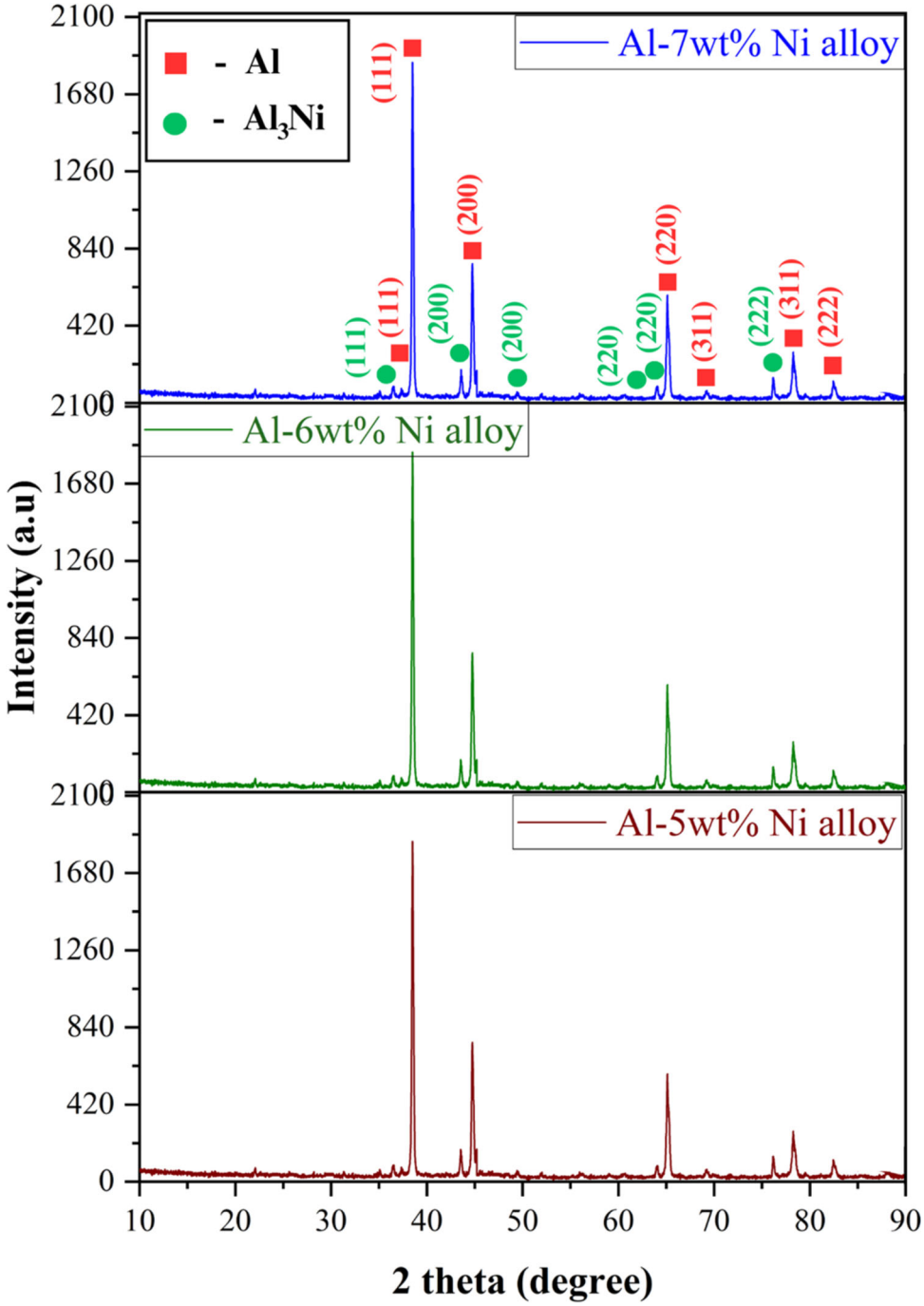

Fig. 3 XRD graphs of investigated Al-Ni alloys

nickel concentrations. Similarly, the yield strength, which represents the stress required to initiate plastic deformation, also increases with rising nickel content due to the same strengthening mechanisms responsible for the UTS increase. The Al-6 wt.% Ni alloy shows a 0.58% higher yield strength than the Al-5 wt.% Ni alloy, and the Al-7 wt.% Ni alloy exhibits a more pronounced 1.34% higher yield strength than the Al-6 wt.% Ni alloy (Figure 4). This further supports the idea of a more potent strengthening effect at the higher nickel contents. The slight decrease in elongation with increasing nickel content, particularly noticeable in the Al-7 wt.% Ni alloy, is a common trade-off observed in strengthened alloys.

While the addition of nickel and the formation of Al_3Ni enhance strength and hardness, they also reduce the ductility of Al-Ni alloy, which is its ability to deform plastically before fracture. This is reflected by the lower elongation values and generally shows a decrease in ductility. The UTS and yield strength values are also consistent, showing an increasing trend with higher nickel content due to the reinforcement by the Al_3Ni intermetallic phase. The elongation values are also within the expected range and show the typical decrease in ductility with increasing nickel content due to the presence of the brittle Al_3Ni phase (Ref 19, 34-36).

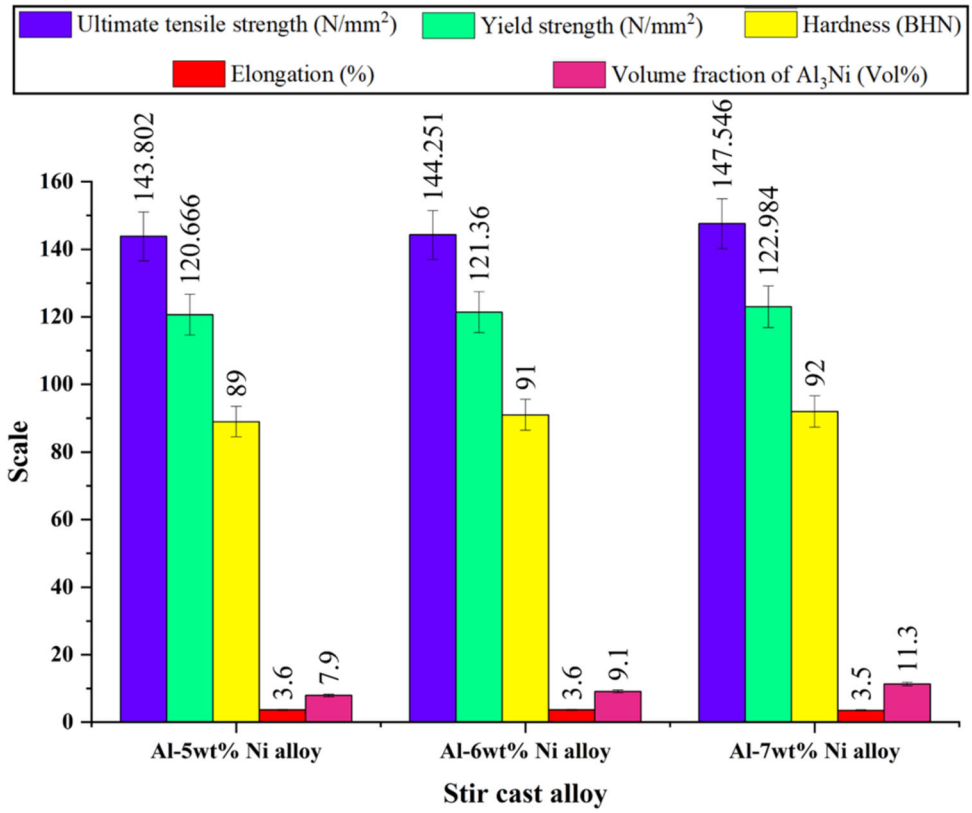

Fig. 4 Measured properties of investigated Al-Ni alloys

3.3 Multi-objective Optimization of Wear Behavior of Al-Ni Alloys

In this study, the wear resistance of the stir cast Al-Ni alloys is optimized using a powerful statistical approach termed the Taguchi method. As an organized approach to experimental design, this technique makes it easy for researchers to do experiments and determine how different factors affect an outcome (Ref 37). Here in the study, the basis of interest is the least friction and wear; these two are very important to improving the performance of materials for tribological applications. For their analysis, the investigation selected the "smaller-the-better" quality characteristic because it is beneficial to minimize the coefficient of friction and the specific wear rate of the Al-Ni alloys. The premise of this attribute is to reduce deviation from an optimal value of zero, which signifies low friction and wear. To quantify this, treated as a smaller-the-better signal-to-noise (S/N) ratio and quantified the results using a particular equation for S/N ratio-based data transform into a metric of how close the results are to the desired results.

By conducting experiments based on a Taguchi orthogonal array, systematically varied factors such as nickel content, sliding speed, applied load, and sliding distance. This enabled to efficiently explore the interaction of these factors with the wear behavior of Al-Ni alloys on an individual and combined basis. Through the analysis of the *S*/*N* ratios for both COF and specific wear rate, determined the optimum combination of the factor levels that caused the lowest friction and wear, thereby improving the wear resistance of the Al-Ni alloys. The smaller-the-better quality characteristic is expressed in Eq 6 (Ref 38).

$$S/N = -10\log\left[\frac{1}{n}\sum_{i=1}^{n} y_i^2\right] \quad \text{(Eq 6)}$$

where, n is the number of observations, and y_i is observed data of the ith experiment.

The observed responses for the various factor combinations are presented in Table 4. Prof. Deng's gray technique has been useful for handling incomplete, inaccurate, or otherwise problematic data in system models. In data, "gray relations" denote incomplete connections. Complex issues, including interrelationships between multi-objective features, are efficiently resolved using gray relational analysis. A single gray relational grade is generated from the optimization of multi-performance criteria throughout the investigation. The optimal combination of the control elements on multi-objective characteristics was determined in this experiment using GRA. The control factors are nickel content, applied load, sliding velocity, and sliding distance. Implementation of the GRA approach yielded the data shown in Table 5, namely, the gray relational grades acquired from pre-processed replies. It is necessary to concurrently determine the impact of each factor on the output characteristics while minimizing the particular wear rate and coefficient of friction.

Table 6 shows the response for means, allowing the most influential factor variable for specific wear rate to be determined. Figure 5 graphically presents the impact of the four factors on the means. According to Table 6 and Fig. 5, the control factors with higher mean values provide the optimal factor variant. The analysis of the results indicates the factor

Table 4 The observed responses for experimental combination of factors

	Factors				Responses		
Exp. run	Ni element, N	Sliding speed, S	Applied load, A	Sliding distance, D	Wear loss, grams	Specific wear rate (SWR), $\times 10^{-5}$ mm^3/Nm	Coefficient of friction (COF)
1	5	1	10	500	4.108	5.842	0.465
2	5	1	20	1000	4.033	7.427	0.325
3	5	1	30	1500	3.941	4.289	0.121
4	5	2	10	1000	9.991	14.699	0.564
5	5	2	20	1500	3.867	4.748	0.156
6	5	2	30	500	4.123	10.124	0.458
7	5	3	10	1500	3.564	8.751	0.523
8	5	3	20	500	7.562	13.119	0.557
9	5	3	30	1000	3.698	4.54	0.198
10	6	1	10	1000	5.325	12.233	0.61
11	6	1	20	1500	3.897	4.777	0.201
12	6	1	30	500	3.992	9.788	0.662
13	6	2	10	1500	3.672	9.003	0.629
14	6	2	20	500	3.568	13.121	0.547
15	6	2	30	1000	14.765	30.262	0.795
16	6	3	10	500	14.329	31.841	0.745
17	6	3	20	1000	4.442	8.168	0.432
18	6	3	30	1500	4.813	3.934	0.265
19	7	1	10	1500	2.892	7.073	0.527
20	7	1	20	500	8.981	14.604	0.421
21	7	1	30	1000	5.932	7.254	0.487
22	7	2	10	500	25.684	41.702	0.758
23	7	2	20	1000	6.965	12.775	0.647
24	7	2	30	1500	5.030	4.1	0.199
25	7	3	10	1000	10.239	22.887	0.589
26	7	3	20	1500	4.991	6.103	0.337
27	7	3	30	500	9.871	16.804	0.614

combination for minimal multi-objective characteristics includes a nickel element weight percentage of 5 wt.%, a sliding speed of 1 m/s, an applied load value of 30 N, and a sliding distance of 1500 m. Additionally, the ranking in the table reveals the most influential factors are sliding distance, followed by applied load, nickel element, and sliding speed. The levels of the optimal control factor variant are N1S1A3D3, meaning the first two factors are at the first level and the other two are at the third level.

Results from analyzing the gray relational grade values in Table 4 show that the best factor-level combination is characterized by the greatest GRG value. Figure 6 further supports this, demonstrating that experiment 3 has the highest GRG (0.9908), which corresponds to a nickel content (N) of 5 wt.%, applied load (A) of 30 N, sliding speed (S) of 1 m/s, and sliding distance (D) of 1500 m. Stir cast Al-Ni alloys design their dry sliding wear process to minimize the specific wear rate and coefficient of friction. This ideal factor combination seeks to do just that. The response table for means of GRG provides a better understanding of the factors affecting the wear performance of stir cast Al-Ni alloys. In particular, it is observed that as nickel content increases from the lowest level to the highest level, the mean response value decreases, indicating that a lower Ni content helps in minimizing wear (Ref 34, 39). In contrast, sliding speed exhibits a negligible impact, with only a slight decrease in mean response as speed increases, implying its effect is not significant within the tested range. Conversely, both applied load and sliding distance show a direct correlation with wear. The mean response value increases as the load ramp increases from the lowest to the highest load level, thus implying higher loads translate into greater wear. It is observed that this analogous increase in the wear with increased sliding distance also confirms these factors as being essential in controlling wear behavior. The findings show the general importance of optimizing the nickel content and highlight the importance of the effects of applied load and sliding distance on the wear characteristics of Al-Ni alloys.

Results of the ANOVA of dry sliding wear in stir cast Al-Ni alloys for multi-objective optimization (Table 7) show that applied load and sliding distance have a significant impact on wear behavior. The applied load has a high F-value of 45.30 and a low p-value of 0.002, indicating that increased loads lead to greater wear. Similarly, the sliding distance has a high F-value of 62.78 and a low p-value of 0.001, suggesting that longer sliding distances also contribute to increased wear. The Ni element content, with an F-value of 6.60 and a p-value of 0.007, shows a significant influence, albeit to a lesser degree. This suggests that a higher nickel content might potentially minimize wear. On the other hand, the high p-value of 0.348 and the low F-value of 1.12 indicate that sliding speed has a minimal impact. These findings emphasize the importance of controlling applied load and sliding distance to mitigate wear while potentially increasing nickel content for improved performance, as sliding speed appears to play a minimal role under the tested conditions. Further, the regression equation

Table 5 Gray relational grades obtained through pre-processed responses

	Pre-processed responses (Ideal = 1)		Gray relational coefficient (GRC) (Ideal = 1)			
Exp. run	SWR	COF	SWR	COF	Gray relational grade (GRG)	Order
1	0.9495	0.48961	0.9082	0.4949	0.7015	9
2	0.9075	0.69733	0.8439	0.6229	0.7334	8
3	0.9906	1.00000	0.9815	1.0000	0.9908	1
4	0.7150	0.34273	0.6369	0.4321	0.5345	22
5	0.9784	0.94807	0.9587	0.9059	0.9323	2
6	0.8361	0.50000	0.7531	0.5000	0.6266	13
7	0.8725	0.40356	0.7968	0.4560	0.6264	14
8	0.7568	0.35312	0.6728	0.4360	0.5544	19
9	0.9840	0.88576	0.9689	0.8140	0.8915	4
10	0.7803	0.27448	0.6947	0.4080	0.5513	20
11	0.9777	0.88131	0.9573	0.8082	0.8827	5
12	0.8450	0.19733	0.7634	0.3838	0.5736	17
13	0.8658	0.24629	0.7884	0.3988	0.5936	15
14	0.7568	0.36795	0.6727	0.4417	0.5572	18
15	0.3029	0.00000	0.4177	0.3333	0.3755	26
16	0.2611	0.07418	0.4036	0.3507	0.3771	25
17	0.8879	0.53858	0.8169	0.5201	0.6685	10
18	1.0000	0.78635	1.0000	0.7006	0.8503	6
19	0.9169	0.39763	0.8575	0.4536	0.6555	12
20	0.7175	0.55490	0.6390	0.5290	0.5840	16
21	0.9121	0.45697	0.8505	0.4794	0.6649	11
22	0.0000	0.05490	0.3333	0.3460	0.3397	27
23	0.7659	0.21958	0.6811	0.3905	0.5358	21
24	0.9956	0.88427	0.9913	0.8120	0.9017	3
25	0.4982	0.30564	0.4991	0.4186	0.4589	24
26	0.9426	0.67953	0.8970	0.6094	0.7532	7
27	0.6592	0.26855	0.5947	0.4060	0.5004	23

Table 6 Response table for means of GRG

Level	Ni element, N	Sliding speed, S	Applied load, A	Sliding distance, D
1	0.6961*	0.6680*	0.5014	0.4987
2	0.6395	0.6359	0.6890	0.6378
3	0.5993	0.6312	0.7446*	0.7985*
Delta	0.0968	0.0368	0.2432	0.2998
Rank	3	4	2	1

*Statistical significance in favor of better multi-objective performance.

developed for the multi-objective characteristic of Al-Ni alloys is given in equation (7).

$$\begin{aligned}\text{Regression equation of GRG} = {} & 0.429256 \\ & - (0.0484031 \times \text{ Ni element (N)}) \\ & - (0.0184034 \times \text{ Sliding speed (S)}) \\ & + (0.0121595 \times \text{ Applied load (A)}) \\ & + (0.000299785 \times \text{ Sliding distance (D)})\end{aligned} \quad \text{(Eq 7)}$$

In order to assess the linear regression model's assumptions, the residual plots were shown (Fig. 7). The histogram and normal probability plot of residuals show that the normality condition is met, suggesting that residuals are almost normally distributed. The lack of a clear trend in the plot of fitted values versus residuals suggests that the homoscedasticity condition is probably satisfied. This means that the residuals' variance remains constant over the range of fitted values. However, the plot of residuals versus observation order reveals a potential pattern, which suggests a non-violation of the independence assumption. The provided main effects plot for the means visualizes the impact of the four factors on the specific response variable (Fig. 5). The analysis reveals that as the nickel element content increases, the mean response value decreases. This suggests that increasing the nickel content (from 5 to 7 wt.%) might be advantageous for the wear behavior of the stir cast Al-Ni alloys. In contrast, the effect of sliding speed (1 to 3 m/s) appears to be minimal. There is a slight decrease in the mean response as the speed increases, but the difference is not statistically significant within the tested range. This implies that sliding speed has a negligible impact on the wear characteristics of the alloys. The findings reveal that the mean response value rises in relation to the applied load, which ranges from 10 to 30 N. This indicates that higher loads lead to increased wear, which is an important consideration for the optimization of the dry sliding wear process. Similarly, increasing the sliding

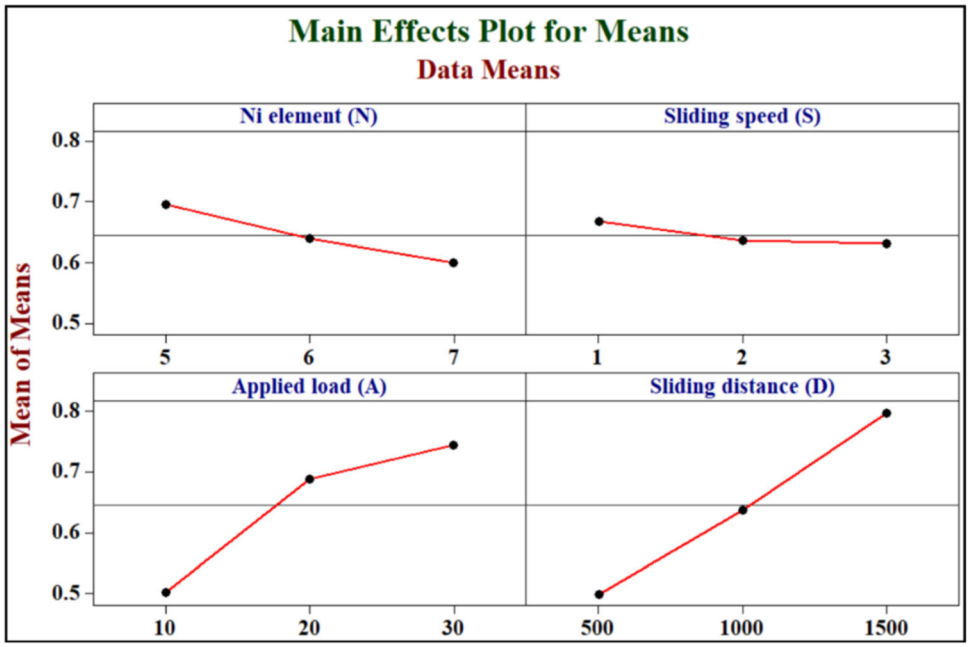

Fig. 5 Main effects plots for Means of this experimentation

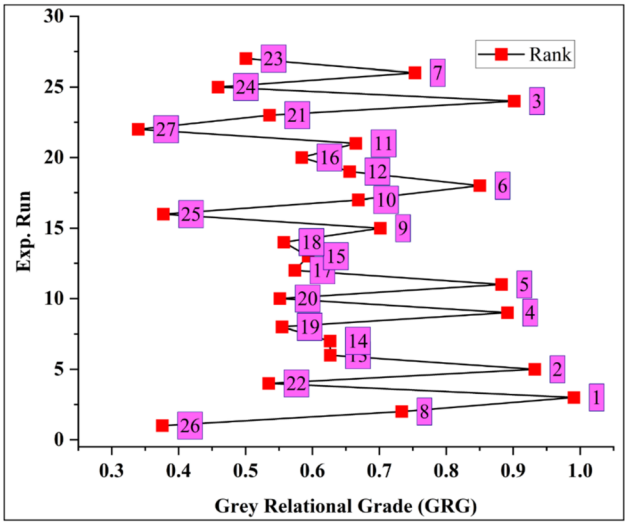

Fig. 6 Ranks assigned to GRG values of this experimentation

distance (from 500 to 1500 m) results in a higher mean response value, suggesting that longer sliding distances contribute to increased wear. All things considered, the results indicate that the nickel element content is not only the single most important factor influencing wear behavior, with materials having significant nickel concentrations benefiting from lower wear rates. On the flip side, sliding speed has no effect on wear behavior within the range of tests, although both a greater applied load and sliding distance lead to increased wear.

Among the many variables influencing the dry sliding wear behavior of stir cast Al-Ni alloys, sliding distance stands out as the most important, explaining 50.3% of the total variance (Fig. 8). This underscores the significant impact of increased sliding distances on wear. Applied load is the next most influential factor, contributing 36.3% and highlighting its critical role in escalating wear under higher loads. In contrast, the nickel element content exhibits a less pronounced, yet notable, influence, contributing 7.2% to the overall variation. Sliding speed, however, shows a negligible impact, comprising only 0.9% of the total variation within the tested range. Collectively, these findings emphasize that sliding distance and applied load are the primary determinants of wear in Al-Ni alloys, while the nickel content also plays a relevant, albeit less dominant, role. Sliding speed appears to have a minimal effect on the wear characteristics under the examined conditions.

To ensure the correctness of the analysis, a confirmation test had been performed when the ideal values of the control factors were obtained. This validation test for the dry sliding process of Al-Ni alloys employed the best possible levels of control factors to verify the response characteristics of the output. Equation 8 was used to calculate the predicted value of the gray relational grade (Ref 40).

$$\gamma_p = \gamma_m + \sum_{k=1}^{n} (\gamma_k - \gamma_m) \qquad \text{(Eq 8)}$$

where γ_p represents the predicted GRG, γ_m stands for the sum of all GRG values, γ_k denotes the mean GRG value at the optimal level, and k is the count of dry sliding process factors. Table 8 displays the comparison of the experimental and predicted GRG values using the ideal factor levels; the predicted value is 0.9956 and the observed value is 0.8726, with a discrepancy of 0.1230. In terms of dry sliding performance, this means that the stir cast Al-Ni alloys are 14.1% better (Table 8). Between the Rank 1 combination factor setting and the optimal wear test factor setting, there is an 86.8% improvement in the GRG. This proves the validity of the approach used to find the best analysis factors with many performance metrics. At the 95% confidence level, all of the residuals follow a normal distribution along the straight line, as shown in Fig. 7, which is the normal probability plot of the GRG. SEM images of Al-5 wt.% Ni alloy dry sliding wear test pins corresponding to experimental run 1 ($N1$ = 5 wt.% Ni,

Table 7 Analysis of variance for GRG

Source	*DF*	Seq SS	Adj SS	Adj MS	*F*	*P*
Ni element (N)	2	0.042574	0.042574	0.021287	6.60	0.007
Sliding speed (S)	2	0.007223	0.007223	0.003611	1.12	0.348
Applied load (A)	2	0.292324	0.292324	0.146162	45.30	0.002
Sliding distance (D)	2	0.405117	0.405117	0.202559	62.78	0.001
Error	18	0.058074	0.058074	0.003226		
Total	26	0.805313				
S = 0.0568008		R-Sq = 92.79%		R-Sq(adj) = 89.58%		

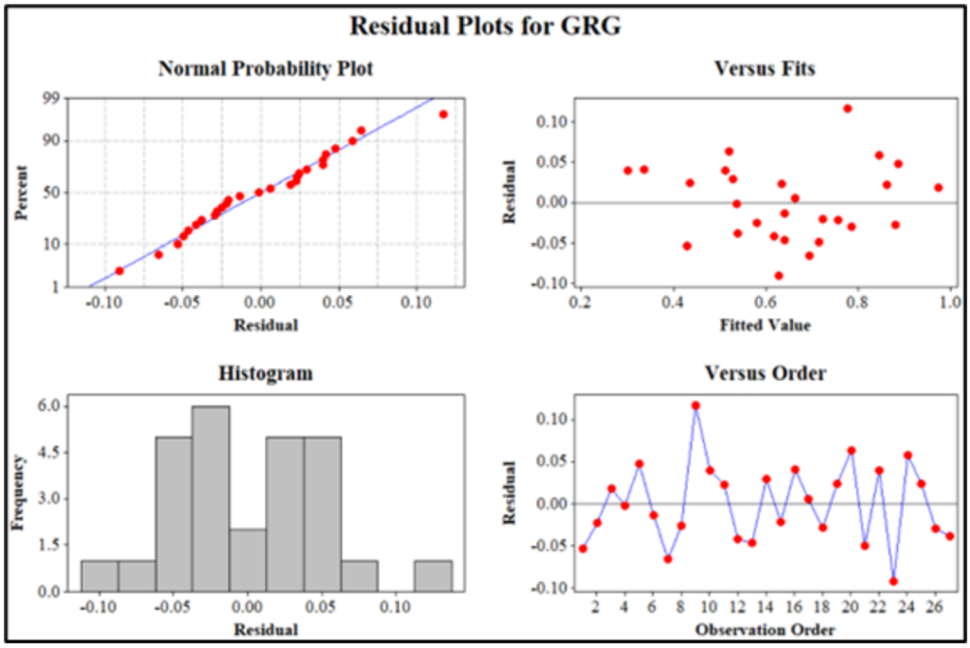

Fig. 7 Residual plots for GRG of this experimentation

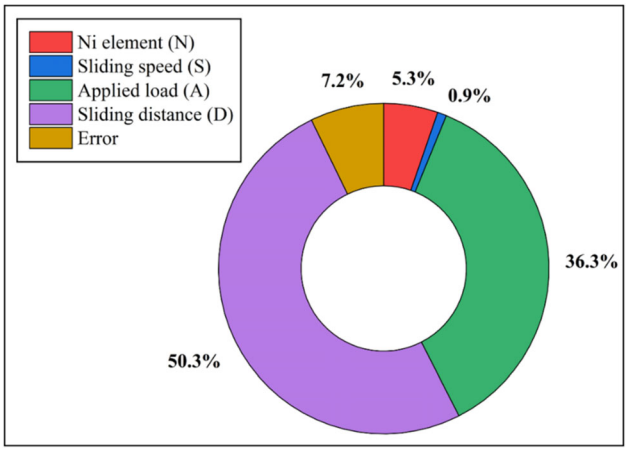

Fig. 8 Contribution (%) of each control factor toward the multi-objective characteristic of Al-Ni alloys

$S1$ = 1 m/s, $A1$ = 10 N, $D1$ = 500 m) and the optimal wear test combination ($N1$ = 5 wt.% Ni, $S1$ = 1 m/s, $A3$ = 30 N, $D3$ = 1500 m) reveal surface features, including surface roughness, plastic deformation, microcracks, and wear debris (Fig. 9). The observed wear features suggest that the dominant wear mechanisms are abrasive wear, adhesive wear, and fatigue wear. Abrasive wear occurs as hard phases in the wear track plow through the softer material, leading to material removal. Adhesive wear results from adhesion between the contacting surfaces, causing material transfer and the formation of wear debris (Ref 41). Fatigue wear is driven by repeated stress cycles at the contact surface, which initiate and propagate cracks, resulting in material loss. SEM image for experimental run 1 exhibits severe surface damage, with deeper grooves, pits, and more pronounced plastic deformation. Numerous microcracks and larger wear debris particles are also observed (Fig. 9a). Interestingly, the image for the optimal wear test combination shows moderate surface damage, with some scratches, grooves, and plastic deformation. Microcracks and wear debris are still present (Fig. 9b). It has been observed that the applied load escalates the contact pressure, leading to greater plastic deformation, material removal, and the generation of larger wear debris. Sliding distance extends the wear process in pins, resulting in more extensive damage, microcrack formation, and propagation.

A detailed correlation between the microstructural characteristics of the Al-5 wt.% Ni alloy and its observed wear behavior reveals that the distribution and morphology of Al_3Ni

Table 8 Initial and optimum wear test outcomes

	Initial factors combination (Exp. Run 1)	Optimal wear test factors	
		Predicted	Experimental
Combination	N1S1A1D1	N1S1A3D3	N1S1A3D3
Specific Wear Rate (SWR) ($\times 10^{-5}$ mm^3/Nm)	30.262	…	3.934
Coefficient of Friction (COF)	0.795	…	0.124
GRG	0.7015	0.8726	0.9956
Improvement of the GRG = 0.1230 (14.1% of improvement observed).			

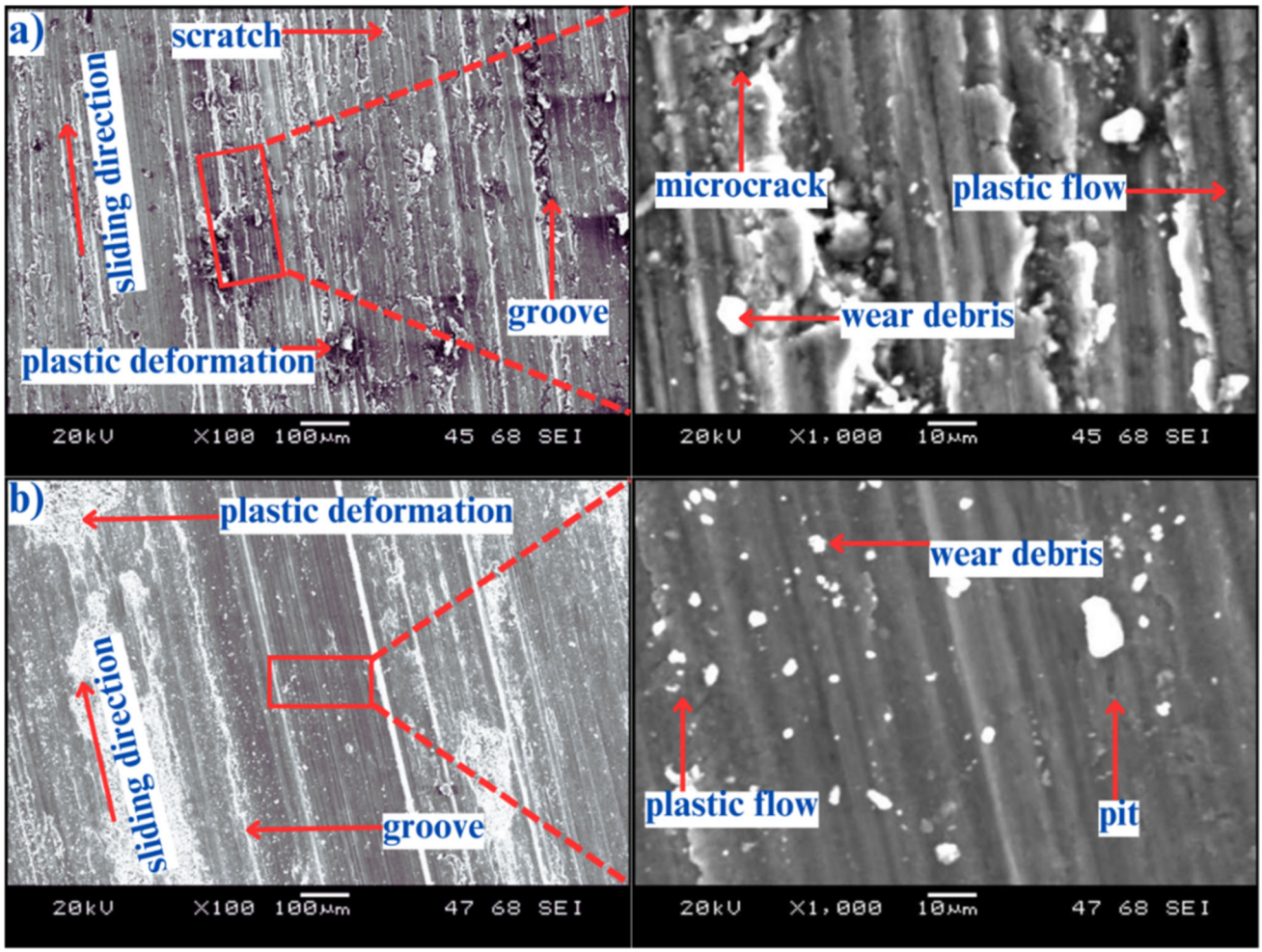

Fig. 9 Worn SEM images of (a) Exp. Run 1 combination (N1S1A1D1), and (b) Optimal wear test combination (N1S1A3D3)

intermetallics play a crucial role in governing the dominant wear mechanisms. The uniform dispersion of fine Al_3Ni particles within the α-Al matrix enhances the hardness and load-bearing capacity of the alloy, which helps in resisting surface damage during sliding. However, due to the relatively low volume fraction of Al_3Ni (7.9 vol.%) and the predominance of softer α-Al dendrites, the alloy still remains partially vulnerable to adhesive and fatigue wear. The SEM analysis of the worn surface from experimental run 1 (low load and short sliding distance) indicates severe surface damage, with deep grooves and pits formed primarily due to adhesive interactions and micro-plowing by hard counterface asperities. These features suggest that the α-Al matrix undergoes significant plastic deformation under contact stress, promoting material transfer and the formation of larger wear debris (Fig. 9a)). Furthermore, the presence of microcracks and fragmented debris implies that cyclic stresses at the contact interface led to fatigue crack initiation and propagation, which is consistent with fatigue wear (Ref 42). In contrast, under the optimal wear test combination (higher load and longer distance), although the wear surface still exhibits plastic deformation and microcracks, the damage is comparatively moderate (Fig. 9b)). This suggests that under increased mechanical and thermal loads, the fine and well-distributed Al_3Ni intermetallics contribute to improved wear resistance by supporting the applied load, reducing localized deformation, and hindering crack propagation (Ref

43). Therefore, the microstructural refinement and controlled distribution of intermetallics directly influence the transition from severe adhesive/fatigue wear to a more controlled abrasive wear regime, underscoring the importance of tailoring the microstructure to enhance wear performance in Al-Ni alloys.

4. Conclusions

This study investigated the multi-objective optimization of dry sliding wear control factors for stir cast Al-Ni alloys using the Taguchi-Gray relational approach. The key findings are:

- Increasing Ni content in the Al-Ni alloy leads to a higher volume fraction of the Al_3Ni intermetallic phase, which helps improve strength and hardness.
- XRD and EDS analyses confirm the presence and increasing volume fraction of the Al_3Ni phase with higher Ni content, supporting the observed microstructural changes.
- The density of stir cast Al-Ni alloys increases with higher Ni content due to the higher atomic weight of Ni and its substitution within the aluminum crystal lattice, contributing to enhanced mechanical properties.
- The hardness of the Al-Ni alloys rose as the Ni concentration increased, with the Al-6 wt.% Ni alloy showing 2.22% more hardness than the Al-5 wt.% Ni alloy. This is mainly because of the solid solution strengthening and the emergence of hard Al_3Ni intermetallic compounds.
- The ultimate tensile strength of the Al-Ni alloys increased with increasing Ni content, with the Al-7 wt.% Ni alloy exhibiting a 2.3% higher UTS than the Al-6 wt.% Ni alloy, attributed to solid solution strengthening and the presence of hard Al_3Ni intermetallic phases.
- Sliding distance (50.3%) and applied load (36.3%) were identified as the most significant factors influencing wear behavior. Nickel content played a less dominant but notable role (7.2%), with higher content generally leading to benefit wear resistance. Sliding speed had a negligible impact (0.9%) within the tested range. SEM analysis of worn surfaces revealed adhesive wear, abrasive wear, and fatigue wear as the dominant wear mechanisms.
- Optimization through Taguchi-GRA achieved a 14.1% improvement in dry sliding performance (GRG difference of 0.1230). The GRG improved by 86.8% from the initial factor setting to the optimal wear test setting.

In summary, the Taguchi-Gray relational strategy was shown to be beneficial in this work for improving the dry sliding wear performance of stir cast Al-Ni alloys. Future scope and application of this study include design and development of Al-Ni based wear-resistant alloys for automotive, and aerospace applications, in which high-strength, lightweight, and superior tribological performance are critical requirements.

References

1. S. Limin, Investigation of Tool Wear and Surface Roughness When Turning Titanium Alloy (Ti6Al4V) under Different Cooling and Lubrication Conditions, *Ferroelectrics*, 2018, **526**(1), p 199–205. https://doi.org/10.1080/00150193.2017.1391003
2. V. Güther, M. Allen, J. Klose, and H. Clemens, Metallurgical Processing of Titanium Aluminides on Industrial Scale, *Intermetallics*, 2018, **103**, p 12–22. https://doi.org/10.1016/j.intermet.2018.09.006
3. B. Callegari, T.N. Lima, and R.S. Coelho, The Influence of Alloying Elements on the Microstructure and Properties of Al-Si-Based Casting Alloys: A Review, *Metals*, 2023, **13**(7), p 1174. https://doi.org/10.3390/met13071174
4. F.G. Coury, C.S. Kiminami, W.J. Botta, C. Bolfarini, and M.J. Kaufman, Design and Production of Al-Mn-Ce Alloys with Tailored Properties, *Mater. Des.*, 2016, **110**, p 436–448. https://doi.org/10.1016/j.matdes.2016.08.008
5. A. Shang, B. Stegman, K. Choy, T. Niu, C. Shen, Z. Shang, X. Sheng, J. Lopez, L. Hoppenrath, B.P. Zhang, H. Wang, P. Bellon, and X. Zhang, Additive Manufacturing of an Ultrastrong, Deformable Al Alloy with Nanoscale Intermetallics, *Nat. Commun.*, 2024, **15**, p 1. https://doi.org/10.1038/s41467-024-48693-4
6. C. Da Costa, W. Zapata, F. Velasco, J. Ruiz-Prieto, and J. Torralba, Wear Behaviour of Aluminium Reinforced with Nickel Aluminide MMCs, *J. Mater. Process. Technol.*, 1999, **92**, p 66–70. https://doi.org/10.1016/s0924-0136(99)00213-7
7. S. Bhowmick, F. Muhaffel, G. Sun, H. Cimenoglu, and A.T. Alpas, Role of Counterfaces with DLC and N-Based Coatings on Frictional Behaviour of AZ31 Magnesium Alloy Subjected to Plasma Electrolytic Oxidation (PEO) Process, *Surf. Coat. Technol.*, 2020, **397**, 125997. https://doi.org/10.1016/j.surfcoat.2020.125997
8. X. Song, Y. Li, and F. Zhang, Microstructure and Mechanical Properties of Nb- and Mo-Modified NiTi–Al-Based Intermetallics Processed by Isothermal Forging, *Mater. Sci. Eng. A*, 2013, **594**, p 229–234. https://doi.org/10.1016/j.msea.2013.11.070
9. A. Saiyathibrahim, S. Santhosh, G.R. Kumar, and S.B. Kumar, Influence of Nickel on the Microstructural Evolution and Mechanical Properties of LM6-Alloy-Based Functionally Graded Composite tubes, *Materiali in Tehnologije*, 2023, **8**, p 9. https://doi.org/10.17222/mit.2023.799
10. C.A. León-Patiño, E.A. Aguilar-Reyes, E. Bedolla-Becerril, A. Bedolla-Jacuinde, and S. Méndez-Díaz, Dry Sliding Wear of Gradient Al-Ni/SiC Composites, *Wear*, 2013, **301**(1–2), p 688–694. https://doi.org/10.1016/j.wear.2012.11.052
11. R. Kakitani, A.P. Carrara, F.E. Mariani, N.C. Veríssimo, L.C. Casteletti, A. Garcia, and N. Cheung, Tensile, Wear, and Corrosion Behaviors of an In Situ Al–Al3Ni Metal Matrix Composite Solidified Under Different Cooling Rates, *J. Mater. Sci.*, 2023, **58**(21), p 8796–8814. https://doi.org/10.1007/s10853-023-08578-1
12. V. Ganesh, R.R. Tamboli, A.K. Khanra, and S.R. Dey, Structural Characterisation of Unique Core-Shell Shaped Al3Ni2/Al3Ni in-Situ Intermetallic in Al–4Cu-xNi Via Powder Metallurgy (P/M), *Vacuum*, 2023, **213**, 112166. https://doi.org/10.1016/j.vacuum.2023.112166
13. C. Suwanpreecha, P. Pandee, U. Patakham, and C. Limmaneevichitr, New Generation of Eutectic Al-Ni Casting Alloys for Elevated Temperature Services, *Mater. Sci. Eng. A*, 2017, **709**, p 46–54. https://doi.org/10.1016/j.msea.2017.10.034
14. J. Šmalc, A. Zaky, B. Markoli, and R. Šturm, The Impact of Small Zr Addition to Al–Ni Cast Alloy for Elevated Temperature Applications, *J. Mater. Res. Technol.*, 2024, **32**, p 1928–1936. https://doi.org/10.1016/j.jmrt.2024.08.029
15. A. Saiyathibrahim, R. Subramanian, and C.S.J. Samuel, Processing and Properties Evaluation of Centrifugally Castin-Situfunctionally Graded Composites Reinforced with Al3Ni and Si Particles, *Mater. Res. Express*, 2019, **6**(11), 1165a8. https://doi.org/10.1088/2053-1591/ab4c9f
16. A. Saiyathibrahim, V.S. Jatti, P. Dhanapal, and D.G. Mohan, Development and Characterization of In-Situ Nickel Aluminide Reinforced Al-Si Matrix Composites by Stir Casting, *Eng. Rep.*, 2024, **6**(12), e12966. https://doi.org/10.1002/eng2.12966
17. R.S. Yaseen, E. Dwarakadasa, and A.R. Ismail, Subsurface Damage during Dry Sliding Wear of Al-Al3Ni Eutectic Alloy, *Wear*, 1983, **85**(2), p 213–221. https://doi.org/10.1016/0043-1648(83)90065-0
18. N. Srivastava, G. Chaudhari, and M. Qian, Grain Refinement of Binary Al-Si, Al-Cu and Al-Ni Alloys by Ultrasonication, *J. Mater. Process. Technol.*, 2017, **249**, p 367–378. https://doi.org/10.1016/j.jmatprotec.2017.06.024
19. W.R. Osório, L.C. Peixoto, M.V. Canté, and A. Garcia, Microstructure Features Affecting Mechanical Properties and Corrosion Behavior of a Hypoeutectic Al–Ni Alloy, *Mater. Des.*, 2010, **31**(9), p 4485–4489. https://doi.org/10.1016/j.matdes.2010.04.045

20. Y. Chen, W. Gong, and R. Kang, Review and Propositions for the Sliding/Impact Wear Behavior in a Contact Interface, *Chin. J. Aeronaut.*, 2018, **33**(2), p 391–406. https://doi.org/10.1016/j.cja.2018.06.004
21. W. Zhai, L. Bai, R. Zhou, X. Fan, G. Kang, Y. Liu, and K. Zhou, Recent Progress on Wear-Resistant Materials: Designs, Properties, and Applications, *Adv. Sci.*, 2021 https://doi.org/10.1002/advs.202003739
22. V.S. Jatti, R.M. Krishnan, A. Saiyathibrahim, V.G. Preethi, A. Kumar, S. Sharma, S. Islam, D. Kozak, and J. Lozanovic, Predicting Specific Wear Rate of Laser Powder Bed Fusion AlSi10Mg Parts at Elevated Temperatures Using Machine Learning Regression Algorithm: Unveiling of Microstructural Morphology analysis, *J. Mater. Res. Technol.*, 2024, **33**, p 3684–3695. https://doi.org/10.1016/j.jmrt.2024.09.244
23. I.S. Patil, A. A, S.S. Rao, M.A. Herbert, and D.M. Goudar, Experimental Investigation and Optimisation of Mechanical and Microstructure Behaviour of Stir Cast and Hot-Pressed Al-12.5%Si-ZrO2 Composites: Taguchi and Super Ranking Concept, *Adv. Mater. Process. Technol.*, 2021, **8**(3), p 2576–2602. https://doi.org/10.1080/2374068x.2021.1927648
24. K. Gajalakshmi, N. Senthilkumar, and B. Prabu, Multi-response Optimization of Dry Sliding Wear Parameters of AA6026 Using Hybrid Gray Relational Analysis Coupled with Response Surface Method, *Meas. Control.*, 2019, **52**(5–6), p 540–553. https://doi.org/10.1177/0020294019842603
25. M.M. Khan, A. Dey, and M.I. Hajam, Experimental Investigation and Optimization of Dry Sliding Wear Test Parameters of Aluminium Based Composites, *SILICON*, 2022, **14**(8), p 4009–4026. https://doi.org/10.1007/s12633-021-01158-5
26. K. Brunelli, L. Peruzzo, and M. Dabalà, The Effect of Prolonged Heat Treatments on the Microstructural Evolution of Al/Ni Intermetallic Compounds in Multi Layered Composites, *Mater. Chem. Phys.*, 2015, **149**, p 350–358. https://doi.org/10.1016/j.matchemphys.2014.10.028
27. J. Qian, J. Li, J. Xiong, F. Zhang, and X. Lin, In Situ Synthesizing Al3Ni for Fabrication of Intermetallic-Reinforced Aluminium Alloy Composites by Friction Stir Processing, *Mater. Sci. Eng. A*, 2012, **550**, p 279–285. https://doi.org/10.1016/j.msea.2012.04.070
28. G. Crisponi, V.M. Nurchi, M. Crespo-Alonso, and L. Toso, Chelating Agents for Metal Intoxication, *Curr. Med. Chem.*, 2012, **19**(17), p 2794–2815. https://doi.org/10.2174/092986712800609742
29. D. Srinivasan and K. Chattopadhyay, Formation and Coarsening of a Nanodispersed Microstructure in Melt Spun Al–Ni–Zr Alloy, *Mater. Sci. Eng. A*, 1998, **255**(1–2), p 107–116. https://doi.org/10.1016/s0921-5093(98)00769-2
30. G. Miranda, O. Carvalho, D. Soares, and F. Silva, Properties Assessment of Nickel Particulate-Reinforced Aluminium Composites Produced by Hot Pressing, *J. Compos. Mater.*, 2015, **50**(4), p 523–531. https://doi.org/10.1177/0021998315577148
31. J. Esquivel, H.A. Murdoch, K.A. Darling, and R.K. Gupta, Excellent Corrosion Resistance and Hardness in Al Alloys by Extended Solid Solubility and Nanocrystalline Structure, *Mater. Res. Lett.*, 2017, **6**(1), p 79–83. https://doi.org/10.1080/21663831.2017.1396262
32. A.P. Carrara, R. Kakitani, A. Garcia, and N. Cheung, Effect of Cooling Rate on Microstructure and Microhardness of Hypereutectic Al–Ni Alloy, *Arch. Civ. Mech. Eng.*, 2021, **21**, p 1–9. https://doi.org/10.1007/s43452-020-00159-2
33. S. Khaki-Davoudi, S. Nourouzi, and H.J. Aval, Microstructure and Mechanical Properties of AA7075/Al3Ni Composites Produced by Compocasting, *Mater. Today Commun.*, 2021, **28**, 102537. https://doi.org/10.1016/j.mtcomm.2021.102537
34. E. Karakulak, F.G. Koç, R. Yamanoglu, and M. Zeren, Mechanical Properties of Hypoeutectic Al-Ni Alloys with Al3Ni Intermetallics, *Mater. Test.*, 2016, **58**(2), p 117–121. https://doi.org/10.3139/120.110825
35. J.E. Spinelli, M.V. Canté, N. Cheung, N. Mangelinck-Noël, and A. Garcia, Sem Characterization of Al3Ni Intermetallics and Its Influence on Mechanical Properties of Directionally Solidified Hypoeutectic Al-Ni Alloys, *Mater. Sci. Forum*, 2010, **636**, p 465–470. https://doi.org/10.4028/www.scientific.net/MSF.636-637.465
36. P. Tang, S. Lu, H. Chen, F. Mo, and J. Li, Effect of Cerium Addition on Microstructure, Thermal and Rheological Properties of Hypoeutectic Al-Ni Alloy, *Mater. Today Commun.*, 2023, **36**, 106842. https://doi.org/10.1016/j.mtcomm.2023.106842
37. R. Premkumar, R.R. Babu, A. Saiyathibrahim, R.M. Krishnan, R. Vivek, V.S. Jatti, V.S. Rane, and K. Balaji, Optimizing Cutting Parameters for Effective Turning of EN-31 Steel by Utilizing Vegetable-Based Cutting Fluids as a Coolant, *SAE Int. J. Mater. Manuf.*, 2024, **18**(1), p 83–91. https://doi.org/10.4271/05-18-01-0006
38. P. Muthu, Multi Objective Optimization of Wear Behaviour of Aluminium MMCs Using Grey-Taguchi Method, *Manuf. Rev.*, 2020, **7**, p 16. https://doi.org/10.1051/mfreview/2020013
39. R. Yamanoglu, E. Karakulak, M. Zeren, and F.G. Koç, Effect of Nickel on Microstructure and Wear Behaviour of Pure Aluminium Against Steel and Alumina Counterfaces, *Int. J. Cast Met. Res.*, 2013, **26**(5), p 289–295. https://doi.org/10.1179/1743133613Y.0000000066
40. A. Saiyathibrahim, S. Seenivasan, R. Premkumar, and D.G. Mohan, Multi-response Optimization of Wire EDM Parameters for AISI 304 SS Using Grey Relational Analysis, *J. Inst. Eng. Ser. D*, 2025 https://doi.org/10.1007/s40033-025-00882-1
41. T.S. Balaram, K. Muralidharan, U.G.S. Akhilesh, N. Pranav, P. Akash, R.V. Vignesh, R. Senthilkumar, A. Saiyathibrahim, I. Suyambulingam, and S. Siengchin, Influence of Surface Activated Nanophase Pr6O11 Particles on the Physio-Chemical and Tribological Characteristics of SAE20W40 Automotive Lubricant, *Proc. Inst. Mech. Eng. Part D J. Automob. Eng.*, 2024 https://doi.org/10.1177/09544070241254421
42. G. Zhang, J. Tang, K. Yang, R. Wang, Y. Chen, Y. Xiong, and H. Lin, Important Contributions of Metal Interfaces on Their Tribological Performances: From Influencing Factors to Wear Mechanisms, *Compos. Struct.*, 2024, **337**, 118027. https://doi.org/10.1016/j.compstruct.2024.118027
43. M. Mirzaee-Moghadam, H.R. Lashgari, S. Zangeneh, S. Rasaee, M. Seyfor, M. Asnavandi, and M. Mojtahedi, Dry Sliding Wear Characteristics, Corrosion Behavior, and Hot Deformation Properties of Eutectic Al–Si Piston Alloy Containing Ni-Rich Intermetallic Compounds, *Mater. Chem. Phys.*, 2022, **279**, 125758. https://doi.org/10.1016/j.matchemphys.2022.125758